High-Crystalline Single- and Double-Walled Carbon Nanotube Mats Grown by Chemical Vapor Deposition

ARTICLE *in* THE JOURNAL OF PHYSICAL CHEMISTRY C · OCTOBER 2007

Impact Factor: 4.77 · DOI: 10.1021/jp073940f

High-Crystalline Single- and Double-Walled Carbon Nanotube Mats Grown by Chemical Vapor Deposition

G. Lamura* and A. Andreone

CNR-INFM Coherentia and CNISM-Department of Physics, University of Naples Federico II, Piazzale Tecchio 80, 80125, Napoli, Italy

Y. Yang and P. Barbara

Physics Department, Georgetown University, 37th Street and O Street Northwest Washington, D.C. 20057-1228

B. Vigolo, C. Hérold, J.-F. Marêché, and P. Lagrange

Laboratoire de Chimie du Solide Minéral-UMR 7555, Université Henri Poincaré Nancy I, B.P. 239, 54506 Vandoeuvre-lès-Nancy Cedex, France

M. Cazayous and A. Sacuto

Laboratoire Matériaux et Phénomènes Quantiques, Université Paris VII et ESPCI, 10 rue Vauquelin, 75231 Paris, France

M. Passacantando, F. Bussolotti, and M. Nardone

Department of Physics, University of L'Aquila, Via Vetoio, 67010 Coppito, L'Aquila, Italy

Received: May 22, 2007; In Final Form: August 9, 2007

High-quality mats of single- and double-walled carbon nanotubes (SWNT, DWNT) have been grown by the catalytic chemical vapor deposition (CVD) technique. Field-emission scanning electron microscopy (FESEM), high-resolution transmission electron microscopy (HRTEM), and Raman spectroscopy revealed densely packed mats made by SWNTs, a small fraction of DWNTs, and bundles of both. Tube diameters range from 0.72 to 6 nm. Remarkably, Raman measurements show a very high ratio between the G-band and the D-band peak intensities, a clear indication that structural defects and amorphous carbon are largely absent, *without any post-growth treatment*.

1. Introduction

During the last few decades, the increasing attention of industries toward nanoelectronics has raised interest in the study of the electromagnetic properties of artificial nanometric scale media. To this aim, carbon nanotubes (CNTs) have been the object of an intensive research for both applicative and fundamental issues. Among other important applications, these studies allowed the realization of particle and radiation detectors,[1] bolometers,[2,3] superconducting quantum interference devices (SQUID),[4] field-effect transistors (FET)[5] and spin electronic devices.[6] Major interest has been put on single-walled carbon nanotubes (SWNT) because of their excellent mechanical durability as well as their unique structural and electronic properties: SWNTs present a structure of a hollow cylinder of the graphene sheet; thus, their physical properties are determined essentially by how to roll up the graphene sheet or, in short, by their chirality.[7] What makes SWNTs attractive is the simple procedure for their synthesis. Different techniques have been shown promising for the growth of SWNTs: electric arc discharge,[8] laser ablation,[9] catalytic chemical vapor deposition (CVD), plasma-enhanced chemical vapor deposition (PECVD),[10] and very recently also water-assisted CVD for large-scale size-selective CNT forest growth.[11] CVD is presently the most-flexible technique in view of the possible applications of CNTs in nanoelectronics. In the following, we will describe in detail how to obtain large-scale, large amounts of SWNTs in the form of highly compact mat samples with the minimum content of defects and amorphous carbon without any supplementary purification process.[12]

CVD has been widely developed[11,13−15] for large-scale CNTs production and for controlled synthesis directly on semiconductor materials for fundamental and applied research. A proper photolitographic process on the catalyst layer[16] allows the realization of important prototype devices like field-effect transistors,[17] resonators,[18] and chemical sensors.[19,20] Moreover, in the case of bolometric infrared photoresponse devices,[3] this technique can be in principle helpful for depositing large-area SWNT films on whichever substrate.[21]

For the CVD growth of SWNTs, different carbon-containing molecules have been used as feedstock to obtain carbon by a decomposition process: carbon oxide,[22] methane,[23] methane/hydrogen mixtures,[24] ethylene,[25] acetylene,[26−28] benzene,[29] and alcohol.[15] The decomposition is possible at relatively low temperatures (between 700 and 1000 °C) because of the presence of metal catalysts like Fe, Co, Mo, Fe/Mo, Fe/Co, and Ni under

* Author to whom correspondence should be addressed. E-mail: gianrico.lamura@na.infn.it. Tel.:+390817682611. Fax:+390812391821.

10.1021/jp073940f CCC: $37.00
Published on Web 10/03/2007

the form of thin films or nanoparticles. In the former case, an annealing process just before the CNTs growth is needed to clusterize the thin film in a homogeneous dispersion of nanoparticles to favor the CNTs nucleation. Indeed, the size of the synthesized SWNTs depends strongly on the diameter of the metal catalyst nanoparticles used.[11,30−32] It has also been shown that the growth of SWNTs is particularly efficient in the presence of bimetallic catalyst nanoparticles. In the case of Fe/Mo bimetallic catalyst, Al_2O_3[14,23] and zirconia[33] or MgO powders[34] nanoparticles have been used. These nanoparticles play the role of support for the metal catalyst particles.[34]

In this paper, we describe the synthesis of SWNT mat samples by using CVD deposition with methane as the gas feedstock. We will detail the particular procedure that we have used to diffuse bimetallic Fe/Mo catalyst supported by alumina nanoparticles. The synthesized samples have been characterized by field-emission scanning electron microscopy (FESEM), high-resolution transmission electron microscopy (HRTEM), and Raman spectroscopy. These studies reveal the presence of nanotubes with a very high degree of crystallinity and a low percentage of amorphous carbon with the predominance of SWNTs and the presence of DWNTs. The estimated CNT diameter dispersion ranges between 0.72 and 6 nm from HRTEM and Raman measurements.

2. CNT Synthesis

SWNTs and DWNTs were grown by catalytic CVD on Si/SiO_2 substrates using methane as a carbon source. We used *n*-doped Si 7×5 mm^2 chips, covered with a 500-nm-thick SiO_2 layer.[35] In iron-based catalyst solutions, the presence of this layer prevents the iron silicides/di-silicides formation,[36] thus avoiding any reduction of the catalyst amount for the CNTs growth. This improves the density and the quality of the as-grown CNTs and favors the use of these samples for field-effect studies.

The catalyst was a bimetallic suspension of $Fe(NO_3)_3 \cdot 9H_2O$ and $MoO_2(acac)_2$ (acac = acetylacetonate) with alumina (Al_2O_3) nanoparticles in methanol.[14,37] The molar composition was Fe (0.0063 mmol), Mo (0.0019 mmol), and Al_2O_3 (0.079 mmol) in 4 mL of methanol. We halved the concentration of metals and doubled the concentration of alumina nanoparticles in comparison with the values reported in ref 37. This has been done for two reasons: (*i*) the metal concentration must not be too large to prevent the formation of big clusters of catalyst as indeed we noticed in samples made with more-concentrated solutions and as was reported in ref 38. (*ii*) The concentration of alumina nanoparticles has to be relevant in order to improve a more-homogeneous distribution of fine catalyst particles. The solution has been subsequently sonicated, stirred for more than 2 h, and then spin-coated[37] on Si/SiO_2 substrates. The substrates were spinned until the solution dried and subsequently baked in air at 85 °C for 3 min.

All of the samples were placed on a quartz holder positioned at the center of quartz-tube oven and heated up to a temperature of 900 °C for 30 min with Ar gas flowing. This annealing procedure in Ar is important to reduce the active catalyst size, thus increasing the degree of crystallinity of the final CNTs.[34] H_2 was then introduced (633 sccm) for 2 min (pregrowth time) to start the reduction of the catalyst and activate it just before fluxing the feedstock gas.[36] This pregrowth treatment has been kept quite short in time to avoid a too great an increase of iron particle size that may deteriorate the crystalline quality of the produced nanotubes.[34] Methane (2079 sccm) was then added to H_2 for 25 min (growth time). Subsequently, the furnace was cooled in Ar flow alone. We note that the growth temperature at 900 °C is particularly important for several reasons: (*i*) the best-quality SWNTs have been grown usually at temperatures between 800 and 900 °C[34,36,39,40] except in particular cases;[37] (*ii*) minimization of further iron catalyst loss because of FeSi and $FeSi_2$ formation. Fe silicides and di-silicides are stable at temperature lower than 825 °C.[36] (*iii*) The catalitic decomposition of methane is more efficient between 700 and 900 °C because at higher temperatures the production of amorphous carbon, carbon flakes, and carbon fibers is favored.[41] We synthesized 15 mat samples in the same run with the procedure described above. These samples have been characterized by FESEM, HRTEM, and Raman analysis as will be shown in the next sections.

3. Results and Discussion

3.1. Morphology: FESEM Imaging. Field-emission scanning electron microscopy (FESEM) has been done with a Zeiss Supra 55 VP at an accelerating voltage of 0.5 kV to obtain images of the as-grown CNT mat sample surfaces. All of the samples present very similar morphological properties, in between the limiting cases represented by the two samples shown in Figure 1. In particular, in Figure 1a and c large magnification images are shown. In the former case, we note the presence of lighter spots not larger than 1−2 μm in diameter that correspond to areas where the mat is less thick. In the latter case, the sample is completely uniform. The same results have been obtained by performing an FESEM scan all over the sample area, proving the high degree of homogeneity. In Figure 1b and d, we show a magnification of Figure 1a and c, respectively. One can note the inner structure of the mat sample: densely packed nanotubes and ropes of nanotubes grown in all spatial directions. This structure is so thick that is not possible to focus on the substrate. A rough estimate of the thickness gives a value between 5 and 10 μm.

3.2. Structure: HRTEM Study. The HRTEM study was carried out by using a 200 CX Philips apparatus at an operating voltage of 200 kV to analyze the structure of the synthesized nanotubes. The observations were performed on a piece of mat taken from the sample volume and deposited on a TEM copper grid. The same analysis has been performed on different samples obtaining reasonably the same results. For seek of clarity, we show in Figure 2 the HRTEM micrographs taken on one of the analyzed samples. This local HRTEM analysis reveals clearly the presence of both SWNTs and DWNTs in the samples, but it does not allow us to precisely determine the quantitative ratio between the two types of carbon nanotubes. However, the observation of numerous zones on the grids leads to say that the SWNTs seem to be predominant. Carbon nanotube walls are imaged quite easily thanks to their low defect level. The length of the observed carbon nanotubes can reach several micrometers. The observed SWNTs are either assembled in bundles of several tens of carbon nanotubes or isolated. Typically the thinnest (from around 1.2 to 2 nm) form bundles, whereas the larger-diameter tubes (from 3 to 6 nm) are often isolated as seen in Figure 2b. DWNTs can also be identified. They form bundles of several DWNTs (Figure 2c) or they are more or less isolated (Figure 2d). The inner diameter and the outer diameter are in the range of 1−2 nm and 2−3 nm, respectively. In addition, HRTEM measurements show typical interlayer spacing of about 0.5 nm. This value is high compared to the 0.34−0.42 nm range reported for DWNTs from HRTEM and Raman spectroscopy.[12,37,42−46] However, recent TEM studies of DWNTs found a wider range of interlayer spacing, from 0.30 to 0.54 nm.[47]

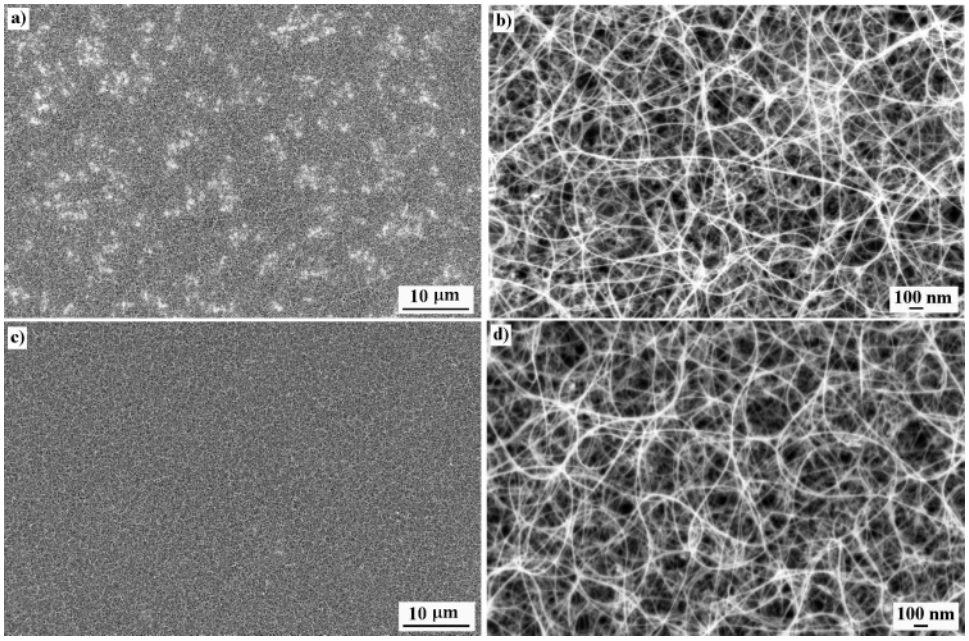

Figure 1. Morphological FSEM characterization: (a) sample 1, low magnification; (b) sample 1, high magnification; (c) sample 2, low magnification; (d) sample 2, high magnification.

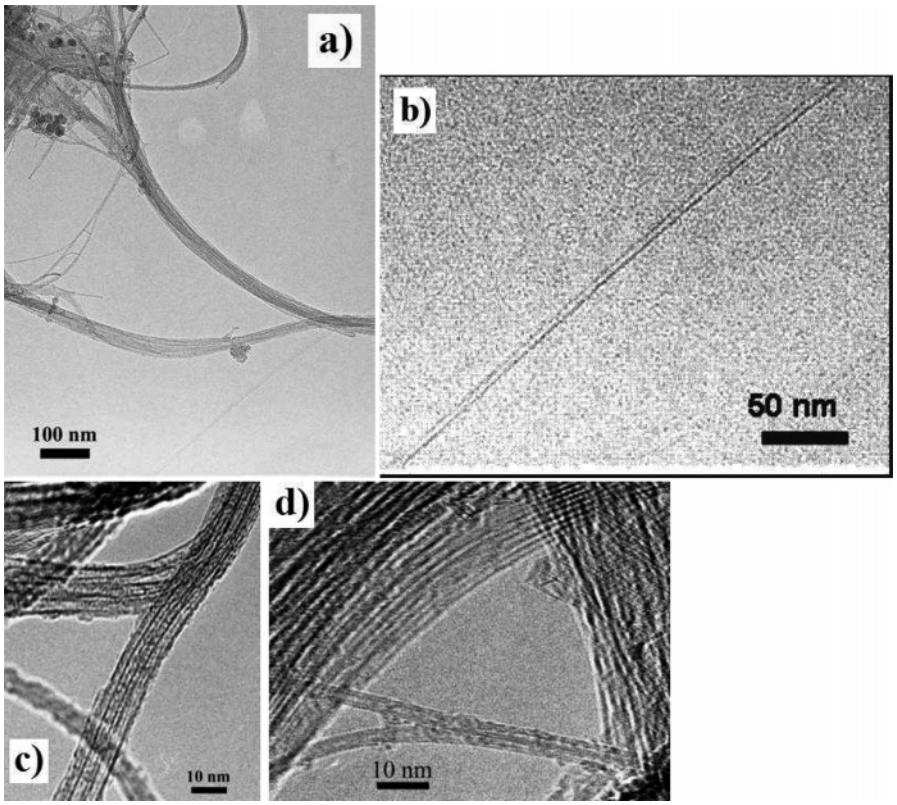

Figure 2. HRTEM micrographs of SWNTs and DWNTs. Isolated and bundled carbon nanotubes can be observed in samples: (a) wide-range image: nanotubes longer than 1 μm are shown; (b) high-magnification image of an isolated SWNT; (c and d) high-magnification image of isolated and bundled DWNTs.

3.3. Structure: RAMAN Spectroscopy. Raman spectroscopy was used to characterize the quality and the average diameter distribution of the as-grown CNTs. The Raman scattering spectra were recorded at room temperature using a triple spectrometer Jobin Yvon T64000 and a LabRam HR High-Resolution Raman Microscope HORIBAJobinYvon. We used the 514.5-nm (2.41 eV) excitation line from a Ar^+-Kr^+ mixed-gas laser and the 632.8-nm (1.96 eV) line from a He−Ne laser. The laser spot size was about 100 μm. The CNTs Raman spectra are characterized by three main signals corresponding to the G band, the D band, and the radial breathing mode (RBM) band. The graphite-like G band appears between 1570 and 1593 cm^{-1} and is due to the tangential phonon modes of a graphene sheet. The feature between 1300 and 1400 cm^{-1} is the D band that indicates the presence of defects and amorphous carbon. The RBM peaks appear from 100 to 500 cm^{-1}, and they are strongly dependent on the nanotube diameter. They are normally not detectable in large-diameter carbon nanotubes (larger than 2 nm)

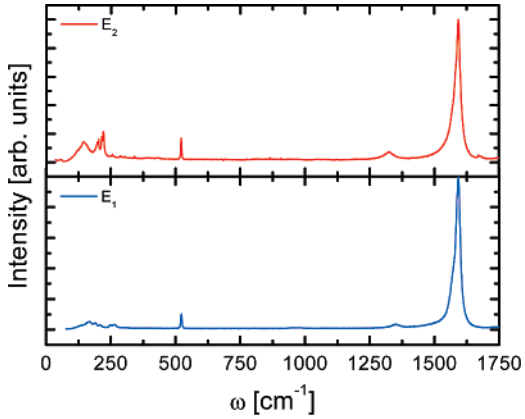

Figure 3. Macro-Raman spectra recorded for two different laser energies, $E_1 = 2.41$ eV on sample 1 and $E_2 = 1.96$ eV on sample 2, respectively.

because of their small Raman scattering cross section.[48,7] RBM peaks are not present in multiwalled nanotubes either for their large radius or because the presence of multi-shells make their Raman spectra more similar to the bulk graphite case.

In Figure 3, we show the recorded macro-Raman spectra on two samples with two different excitation energies: $E_1 = 2.41$ eV and $E_2 = 1.96$ eV, respectively. The high homogeneity put in evidence by the morphological study, and the fact that all of the synthesized samples have been grown in the same run, let us safely generalize these results. In both spectra, RBM signals, a strong G-band, and a very weak D-band peak are clearly visible. We analyze all of these features separately.

RBM Band. The RBM signal yields the diameter distribution. As has been shown previously by TEM characterization, SWNTs, DWNTs, and bundles of SWNTs and DWNTs are present. The tube diameters can be estimated using the following phenomenological relation between the RBM frequency ω_{RBM} (cm^{-1}) and the tube diameter d [45,49−54]

$$\omega_{RBM}(cm^{-1}) = \frac{238}{d(nm)^{0.93}} \quad (1)$$

This relation takes in account a frequency upshift of the RBM modes typically caused by weak van der Waals intertube interactions in bundles with respect to isolated ones.[49,52] It has been assumed that the influence of the van der Waals interactions in the DWNT bundles and in between the outer−inner tube of DWNTs is the same as that in SWNT bundles. In this case, Raman spectra of DWNTs and SWNTs can be interpreted in the same way,[50] that is, as if the sample is made of SWNTs weakly coupled by van der Waals interactions. Using eq 1, the nanotube diameters are estimated from the peaks in the experimental curves in Figure 4, for both laser excitation energies, and they range from 0.72 to 1.60 nm (see Table 1). These results are in good agreement with HRTEM findings, taking into account that CNT diameters larger than 2 nm cannot be put in evidence by this spectroscopic tool. Resonant Raman scattering windows for the interband energies of various SWNTs with different diameters and helicities have been calculated.[50,55] It turns out that one single laser excitation is not sufficient to measure a large range of diameter and helicity distribution. Scans on different locations on the sample surface and different laser excitation energies are necessary to study the distribution of diameter size tubes in carbon nanotube mats. We scanned the mat area at a fixed laser energy and found no substantial differences, thus confirming the high degree of homogeneity.

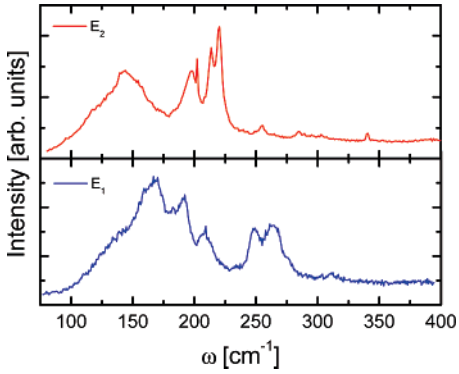

Figure 4. Macro-Raman spectra of the RBM modes recorded for two different laser energies, $E_1 = 2.41$ eV on sample 1 and $E_2 = 1.96$ eV on sample 2, respectively.

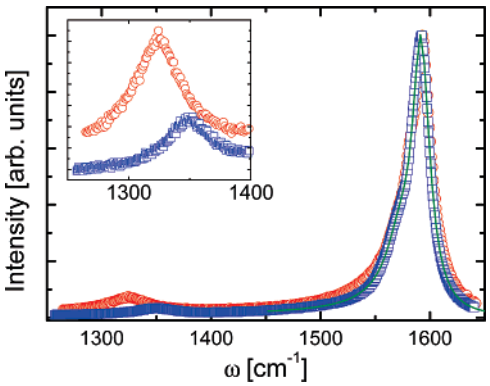

Figure 5. Macro-Raman spectra of the D and G bands recorded for two different laser energies, $E_1 = 2.41$ eV (□) on sample 1 and $E_2 = 1.96$ eV (○) on sample 2, respectively. The spot size is 100 μm for both cases. The continuous line represents a Lorentzian−BWF fit (see text for details). In the inset, we have ploted a magnification of the D bands.

TABLE 1: RBM Frequencies (ω_{Ei}, $i = 1, 2$) versus Diameters (d_i, $i = 1, 2$) for the Two Samples under Test[a]

ω_{E_1}	d_1	ω_{E_2}	d_2
161	1.44	144	1.60
183	1.28	198	1.19
192	1.22	202	1.16
209	1.13	214	1.10
248	0.96	211	1.07
261	0.92	256	0.93
311	0.78	285	0.85
		295	0.82
		341	0.72

[a] The diameters have been calculated by using eq 1.

G Band. The tangential longitudinal and transversal phonon modes (TM) are in the 1570−1593 cm^{-1} range, also named the G band from graphite (the Raman-allowed tangential mode in graphite is observed at 1582 cm^{-1}). In SWNTs, the two most-intense G peaks are labeled G^+ around 1593 cm^{-1}, for C carbon atoms displacements along the tube axis, and G^- around 1570−1585 cm^{-1}, for modes with C displacements along the circumferential direction. The frequency ω_{G^+} is quite independent of tube diameter, whereas ω_{G^-} decreases when decreasing the CNT diameter;[48] that is, the smaller the tube diameter, the softer the tangential vibration in the circumferential direction. The G^- feature is generally broadened for metallic SWNTs in comparison with semiconducting ones. In this case, it is normally fitted by a Breit−Wigner−Fano (BWF) line shape[56] instead of a Lorentzian line shape. In Figure 5, we have plotted the normalized G bands for the two laser energies. Both have mostly

the same shape with a semiconducting-like character. In particular, the G^+ peaks show the same frequency (1593 cm^{-1}) and width: all of these findings on different samples of the same run confirm again the great homogeneity of the synthesized mats.

We consider now the shape of the G peak for the laser energy E_1. In isolated SWNTs, the difference $\Delta\omega = \omega_{G^+} - \omega_{G^-}$ depends on the diameter of the tube; thus, in SWNT/DWNT bundles it will be roughly related to the maximum in the Gaussian diameter distribution of the sample. We have estimated $\Delta\omega = 17$ cm^{-1} performing a Lorentian−BWF fit[57] on the G band at E_1 (see Figure 5). This value indicates that the tubes in resonance with this laser energy are semiconducting with an average diameter around 1.2−1.3 nm (if we refer to the frequency−diameter plot reported in ref 48 for the same laser energy). This is fairly independent of the chirality: nanotubes having any chiral direction with the same diameter exhibit nearly equal G peak splittings.[58]

D Band. The disorder-induced D band in the intermediate range between 1200 and 1400 cm^{-1} is a resonance band mainly originating from defects in tube walls and disordered material surrounding the tubes like amorphous carbon.[45] In order to estimate the degree of crystallinity of CNTs, the ratio between the intensity of the G peak and the D peak $R = I_G/I_D$ has been widely used.[59] In the case of our samples, we found $R = (29 \pm 2)|_{E_1}$. This is to our knowledge *the highest ratio ever reported for as-grown* SWNT/DWNTs by CVD in similar conditions.[12,34,37,39,40,43,45,60−64]

In Figure 5, we note that the D band is located at (1352 ± 2) cm^{-1} with a maximum intensity normalized to the G-band intensity peak of (0.034 ± 0.002) in the case of the Raman spectra taken at E_1, whereas it is at (1324 ± 2) cm^{-1} with a normalized intensity of (0.074 ± 0.002) for the second spectra taken at E_2. It has been predicted theoretically and proved experimentally that on graphitic materials the frequency upshift of the D band increases linearly with the laser excitation energy, E_{LASER}, whereas the intensity of the D band decreases as $I_D \propto (E_{LASER})^{-4}$.[65] In our case, we have $\omega_D^{E_1} - \omega_D^{E_2} = (28 \pm 4)$ cm^{-1}, which is close to 23.6 cm^{-1} predicted value for graphitic materials.[65] Taking into account the above-mentioned E_{LASER} dependence for the D-band intensity and that the G-band intensity is quite insensitive to E_{LASER}, we can calculate the expected variation for the R ratio for two different used laser energies:

$$\left[\frac{I_G}{I_D}\right]_{E_2} = \left[\frac{I_G}{I_D}\right]_{E_1} \cdot \left[\frac{E_2}{E_1}\right]^4 \qquad (2)$$

In our case, the predicted value is $I_G/I_D(E = E_2) = 12.2$, very close to the experimental value (13.4 ± 0.6).

4. Conclusions

We have described a CVD method for the synthesis of SWNT and DWNT on Si/SiO_2 substrates in methane/hydrogen gas flow using a bimetallic Fe/Mo solution as the catalyst. This method allows the production of large-area, high-density, and well-packed CNT mats. Different characterization techniques have been used to study the morphological, structural, and electronic properties of the synthesized samples. FSEM analysis shows that the produced CNTs have a high degree of homogeneity. TEM microscopy reveals that the synthesized nanotubes are in the majority of SWNTs with a non-negligible quantity of DWNTs. They are present both as isolated tubes and arranged in bundles. Raman measurements put in evidence a very high degree of crystallinity and/or a very low content of amorphous carbon without any oxidation process,[12] making these samples extremely attractive for fundamental and applied studies.

Acknowledgment. This work was supported by the NSF (grant nos. DMR0239721 and DMR0521170) and by the AFOSR (grant no. FA9550-06-1-0270). G.L. gratefully acknowledges the financial support of the C.N.R. Short Term Mobility program during his stay at Georgetown University. We are grateful to Dr. V. De Luise and Dr. J. Ghanbaja for their valuable technical assistance.

References and Notes

(1) Wanga, Y.; Kempa, K.; Benham, G.; Li, W. Z.; Kempa, T.; Rybczynski, J.; Herczynski, A.; Ren, Z. F. *Appl. Phys. Lett.* **2004**, *85*, 2607.
(2) Yngvesson, K. S. *Appl. Phys. Lett.* **2005**, *87*, 43503.
(3) Itkis, M. E.; Borondics, F.; Yu, A.; Haddon, R. C. *Science* **2006**, *312*, 413.
(4) Cleziou, J. P.; Wernsdorfer, W.; Bouchiat, V.; Ondarçuhu, T.; Monthioux, M. *Nat. Nanotechnol.* **2006**, *1*, 53.
(5) Martel, R.; Schmidt, T.; Shea, H. R.; Hertel, T.; Avouris, P. *Appl. Phys. Lett.* **1998**, *73*, 2447.
(6) Hueso, L. E.; Pruneda, J. M.; Ferrari, V.; Burnell, G.; Valdés-Herrera, J. P.; Simmons, B. D.; Littlewood, P. B.; Artacho, E.; Fert, A.; Mathur, N. D. *Nature* **2007**, *445*, 410.
(7) Saito, R.; Dresselhaus, G.; Dresselhaus, M. S. *Physical Proprerty of Carbon Nanotubes;* Imperial College Press: London, 1998.
(8) Journet, C.; Maser, W. K.; Bernier, P.; Loiseau, A.; de la Chapelle, M. L.; Lefrant, S.; Deniard, P.; Lee, R.; Fischer, J. E. *Nature* **1997**, *388*, 756.
(9) Thess, A.; Lee, R., P. N.; Dai, H.; Petit, P.; Robert, J.; Xu, C.; Lee, Y. H.; Kim, S. G.; Rinzler, A. G.; Colbert, D. T.; Scuseria, G. E.; Tomaneck, Fischer, J. E. *Science* **1996**, *273*, 483.
(10) Ren, Z. F.; Huang, Z. P.; Xu, J. W.; Wang, J. H.; Bush, P.; Siegal, M. P.; Provencio, P. N. *Science* **1998**, *282*, 1105.
(11) Yamada, T.; Namai, T.; Hata, K.; Futaba, D. N.; Mizuno, K.; Fan, J.; Yudasaka, M.; Yumura, M.; Iijima, S. *Nat. Nanotechnol.* **2006**, *1*, 131.
(12) Sugai, T.; Yoshida, H.; Shimada, T.; Okazaki, T.; Shinohara, H.; Bandow, S. *Nano Lett.* **2003**, *3*, 769.
(13) Dai, H.; Rinzler, A.; Nikolaev, P.; Thess, A.; Colbert, D.; Smalley, R. *Chem. Phys. Lett.* **1996**, *260*, 471.
(14) Kong, J.; Soh, H. T.; Cassell, A. M.; Quate, C. F.; Dai, H. *Nature* **1998**, *395*, 878.
(15) Maruyama, S.; Kojima, R.; Miyauchi, Y.; Chiasi, S.; Kohno, M. *Chem. Phys. Lett.* **2002**, *360*, 229.
(16) Tselev, A.; Hatton, K.; Fuhrer, M. S.; Paranjape, M.; Barbara, P. *Nanotechnology* **2004**, *15*, 1475.
(17) Liu, X.; Lee, C.; Zhou, C.; Han, J. *Appl. Phys. Lett.* **2001**, *79*, 3329.
(18) Peng, H. B.; Chang, C. W.; Aloni, S.; Yuzvinsky, T. D.; Zettl, A. *Phys. Rev. Lett.* **2006**, *97*, 87203.
(19) Kong, J.; Franklin, N. R.; Zhou, C.; Chapline, M. G.; Peng, S.; Cho, K.; Dai, H. *Science* **2000**, *287*, 622.
(20) Zhang, J.; Boyd, A.; Tselev, A.; Paranjape, M.; Barbara, P. *Appl. Phys. Lett.* **2006**, *88*, 123112.
(21) Peng, H. B.; Ristroph, T. G.; Schurmann, G. M.; King, G. M.; Yoon, J.; Narayanamurti, V.; Golovchenko, J. A. *Appl. Phys. Lett.* **2003**, *83*, 4238.
(22) Bronikowski, M. J.; Willis, P. A.; Colbert, D. T.; Smith, K. A.; Smalley, R. E. *J. Vac. Sci. Technol., A* **2001**, *19*, 4.
(23) Cassel, A. M.; Raymakers, J. A.; Kong, J.; Dai, H. *J. Phys. Chem. B* **1999**, *103*, 6484.
(24) Flahaut, E.; Govindaraj, A.; Peigney, A.; Laurent, C.; Rao, N. C. *Chem. Phys. Lett.* **1990**, *300*, 236.
(25) Hafner, J.; Bronikowski, M.; Azamian, B.; Nikolaev, P.; Colbert, P.; Smalley, R. *Chem. Phys. Lett.* **1998**, *296*, 195.
(26) Pan, Z. W.; Xie, S. S.; Chang, B. H.; Wang, C. Y.; Lu, L.; Liu, W.; Zhou, W. Y.; Li, W. Z.; Qian, L. X. *Nature* **1998**, *394*, 631.
(27) Lyu, S. C.; Liu, B. C.; Lee, T. J.; Yang, C. W.; Park, C. Y.; Lee, C. J. *Chem. Commun.* **2003**, 734.
(28) Kasumov, Y. A.; Khodos, I. I.; Volkos, V. T.; Levashov, V. I.; Matveev, V. N.; Shailos, A.; Guéron, S.; Kobylko, M.; Kociak, M.; Bouchiat, H.; Agace, V.; andL. Buchaillot, A. S. R.; Bonnot, A. M. *J. Appl. Phys.,* in press.
(29) Cheng, H.; Li, F.; Su, G.; Dresselhaus, M. *Appl. Phys. Lett.* **1998**, *72*, 3282.
(30) Cheung, C. L.; Kurt, A.; Park, H.; Lieber, C. M. *J. Phys. Chem. B* **2002**, *106*, 2429.
(31) Chenguang, L.; Liu, J. *J. Phys. Chem. B* **2005**, *110*, 20254.
(32) Jeong, G. H.; Suzuki, S.; Kobayashi, Y.; Yamazaki, A.; Yoshimura, H.; Homma, Y. *Appl. Phys. Lett.* **2007**, *90*, 43108.

(33) Han, S.; Yu, T.; Park, J.; Koon, B.; Joo, J.; Hyeon, T.; Hong, S.; Im, J. *J. Phys. Chem. B* **2004**, *108*, 8091.
(34) Ago, H.; Nakamura, K.; Uehara, N.; Tsuji, M. *J. Phys. Chem. B* **2004**, *108*, 18908.
(35) Zhang, J.; Tselev, A.; Yang, Y.; Hatton, K.; Barbara, P.; Shafraniuk, S. *Phys. Rev. B* **2006**, *74*, 155414.
(36) Chakraborty, A. K.; Jacobs, J.; Roberts, C. J.; Hunt, M. R. C. *J. Appl. Phys.* **2006**, *100*, 84321.
(37) Bae, E. J.; Min, Y. S.; Ko, J. H.; Park, W. *Chem. Mater.* **2005**, *17*, 5141.
(38) Liao, X. Z.; Serquis, A.; Jia, Q. X.; Peterson, D. E.; Zhu, Y. T. *Appl. Phys. Lett.* **2003**, *82*, 2694.
(39) Murakami, T.; Mitikami, K.; Ishigaki, A.; Matsumoto, K.; Nishio, K.; Isshiki, T.; Harima, H. *J. Appl. Phys.* **2006**, *100*, 94303.
(40) Harutyunyan, A. R.; Tokune, T.; Mora, E. *Appl. Phys. Lett.* **2005**, *87*, 51919.
(41) Shah, N.; Panjala, D.; Huffmann, G. P. *Energy Fuels* **2001**, *15*, 1528.
(42) Flahaut, E.; Bacsa, R.; Peigney, A.; Laurent, C. *Chem. Commun.* **2003**, *12*, 1442.
(43) Lyu, S. C.; Liu, B. C.; Lee, S. H.; Park, C. Y.; Kang, H. K.; Yang, C.-W.; Lee, C. J. *J. Phys. Chem. B* **2004**, *108*, 2192.
(44) Lyu, S. C.; Liu, B. C.; Lee, C. J.; Kang, H. K.; Yang, C.-W.; Park, C. Y. *Chem. Mater.* **2003**, *15*, 3951.
(45) Osswald, S.; Flahaut, E.; Gogotsi, Y. *Chem. Mater.* **2006**, *18*, 1525 and references therein.
(46) Grüneis, A.; Rümmeli, M.; Kramberger, C.; Barreiro, A.; Pichler, T.; Pfeiffer, R.; Kuzmany, H.; Gemming, T.; Büchner, B. *Carbon* **2006**, *44*, 3177.
(47) Giusca, C. E.; Tison, Y.; Stolojan, V.; Borowiak-Palen, E.; Ravi, S.; Silva, P. *Nano Lett.* **2007**, *7*, 1232.
(48) Jorio, A.; Pimenta, M. A.; Filho, A. G. S.; Saito, R.; Dresselhaus, G.; Dresselhaus, M. S. *New J. Phys.* **2003**, *5*, 139.1.
(49) Rols, S.; Righi, A.; Alvarez, L.; Anglaret, E.; Almairac, R.; Journet, C.; Bernier, P.; Sauvajol, J.; Benito, A.; Maser, W.; Muñoz, E.; Martinez, M.; de la Fuente, G.; Girard, A.; Ameline, J. *Eur. Phys. J. B* **2000**, *18*, 201.
(50) Ci, L.; Zhou, Z.; Yan, X.; Liu, D.; Yuan, H.; Song, L.; Gao, Y.; Wang, J.; Liu, L.; Zhou, W.; Wang, G.; Xie, S.; Tan, P. *J. Appl. Phys.* **2003**, *94*, 5715.
(51) Alvarez, L.; Righi, A.; Rols, S.; Anglaret, E.; Sauvajol, J. L.; Munoz, E.; Maser, W. K.; Benito, A. M.; Martinez, M. T.; de la Fuente, G. F. *Phys. Rev. B* **2001**, *63*, 153401 and references therein.
(52) Henrard, L.; Hernandez, E.; Bernier, P.; Rubio, A. *Phys. Rev. B* **1999**, *60*, R8521.
(53) Alvarez, L.; Righi, A.; Rols, S.; Anglaret, E.; Sauvajol, J. L. *Chem. Phys. Lett.* **2000**, *320*, 441.
(54) Rao, A. M.; Chen, J.; Richter, E.; Schlecht, U.; Eklund, P. C.; Haddon, R. C.; Venkateswaran, U. D.; Kwon, Y. K.; Tomanek, D. *Phys. Rev. Lett.* **2001**, *86*, 3895.
(55) Kataura, H.; Kumazawa, Y.; Maniwa, Y.; Umezu, I.; SIX, S.; Ohtsuka, Y.; Achiba, Y. *Synth. Met.* **1999**, *103*, 2555.
(56) Brown, S. D. M.; Jorio, A.; Corio, P.; Dresselhaus, M. S.; Dresselhaus, G.; Saito, R.; Kneipp, K. *Phys. Rev. B* **2001**, *63*, 155414.
(57) Brown, S. D. M.; Corio, P.; Marucci, A.; Dresselhaus, M. S.; Pimenta, M. A.; Kneipp, K. *Phys. Rev. B* **1999**, *61*, R5137.
(58) Kasuya, A.; Sasaki, Y.; Saito, Y.; Tohji, K.; Nishina, Y. *Phys. Rev. Lett.* **1997**, *78*, 4434.
(59) Delhaes, P.; Couzi, M.; Trinquecoste, M.; Dentzer, J.; Hamidou, H.; Vix-Guterl, C. *Carbon* **2006**, *44*, 3005 and references therein.
(60) Wei, J.; Jiang, B.; Wu, D.; Wei, B. *J. Phys. Chem. B* **2004**, *108*, 8844.
(61) Ramesh, P.; Okazaki, T.; Sugai, T.; Kimura, J.; Kishi, N.; Sato, K.; Ozeki, Y.; Shinohara, H. *Chem. Phys. Lett.* **2006**, *418*, 408.
(62) Zhu, J.; Yudasaka, M.; Iijima, S. *Chem. Phys. Lett.* **2003**, *380*, 496.
(63) Bandow, S.; Takizawa, S.; Hirahara, M.; Yudasaka, M.; Iijima, S. *Chem. Phys. Lett.* **2001**, *337*, 48.
(64) Ren, W.; Cheng, H. M. *J. Phys. Chem. B* **2005**, *109*, 7169.
(65) Sato, K.; Saito, R.; Oyama, Y.; Jiang, J.; Cançado, L.; Pimenta, M.; Jorio, A.; Samsonidze, G.; Dresselhaus, G.; Dresselhaus, M. *Chem. Phys. Lett.* **2006**, *427*, 117.
(66) de Jonge, N.; Allioux, M.; Doytcheva, M.; Kaiser, M.; Teo, K. B. K.; Lacerda, R. G.; Milne, W. I. *Appl. Phys. Lett.* **2004**, *85*, 2607.
(67) Wildöer, J. W. G.; Liesbeth Venema, C.; Rinzler, A. G.; Smalley, R. E.; Dekker, C. *Nature* **1998**, *391*, 59.
(68) Radushkevich, L.; Lukyanovich, V. *Zh. Fiz. Khim.* **1952**, *26*, 88.
(69) Hofer, L.; Sterling, E.; McCartney, J. *J. Phys. Chem.* **1955**, *59*, 1153.
(70) Mannik, J.; Goldsmith, B. R.; Kane, A.; Han, J. *Phys. Rev. Lett.* **2006**, *97*, 16601.
(71) Li, Y.; Kim, W.; Zhang, Y.; Rolandi, M.; Wang, D.; Dai, H. *J. Phys. Chem. B* **2001**, *105*, 11424.
(72) Alvarez, L.; Righi, A.; Guillard, T.; Rols, S.; Anglaret, E.; Laplaze, D.; Sauvajol, J. *Chem. Phys. Lett.* **2000**, *316*, 186.
(73) Jorio, A.; Filho, A. G. S.; Dresselhaus, G.; Dresselhaus, M. S.; Swan, A. K.; Ünlü, M. S.; Goldberg, B. B.; Pimenta, M. A.; Hafner, J. H.; Lieber, C. M.; Saito, R. *Phys. Rev. B* **2002**, *65*, 155412.
(74) Bandow, S.; Chen, G.; Sumanasekera, G. U.; Gupta, R.; Yudasaka, M.; Iijima Eklund, P. C. *Phys. Rev. B* **2002**, *66*, 75416.